JOURNAL OF AIRCRAFT
Vol. 35, No. 4, July–August 1998

Development of Vortex Generator Use for a Transitioning High-Speed Inlet

Bruce J. Wendt*
Modern Technologies Corporation, Middleburg Heights, Ohio 44130-6557
and
Julianne C. Dudek†
NASA Lewis Research Center, Cleveland, Ohio 44135-3191

The development of an effective design strategy for surface-mounted vortex generator arrays in a subsonic diffuser is described in this paper. This strategy uses the strengths of both computational and experimental analyses to determine beneficial vortex generator locations and sizes. A parabolized Navier–Stokes solver, RNS3D, was used to establish proper placement of the vortex generators for reduction in circumferential total pressure distortion. Experimental measurements were used to determine proper vortex generator sizing to minimize total pressure recovery losses associated with vortex generator device drag. The best result achieved a 59% reduction in the distortion index DC60, with a 0.3% reduction in total pressure recovery.

Nomenclature

c = vortex generator chord length
D = cowl diameter or duct width, 25.4 cm
d_o = centerbody or hub diameter, 10.2 cm
h = vortex generator height
p_t = total pressure
q = dynamic pressure
R = cowl radius, 12.7 cm
r = cross-plane radial coordinate
s = vortex generator lateral spacing
x, y, z = Cartesian coordinate system
α = vortex generator angle of attack
δ = boundary-layer thickness
θ = cross-plane circumferential coordinate
ρ = fluid density

Subscripts
min = minimum value
ref = reference conditions at $s/D = -0.5$

Introduction

THE time constraints of an ever-shrinking world are the fundamental driving forces behind recent efforts to expand supersonic cruise flight capability for passenger aircraft. In the U.S. this effort is being conducted through a joint partnership of aerospace industry and NASA in the High Speed Research program. Current examples of supersonic cruise aircraft, the Russian Tu-144 and the Anglo-French Concorde, are products of extensive research efforts culminating nearly 30 years ago. The challenge today, for aerospace engineers participating in NASA's High Speed Research program, is to develop technology for a supersonic flight system that is reliable, efficient, and environmentally acceptable in such a manner that the focus of this effort, a High Speed Civil Transport, will be a frequently flown and profitable aircraft in a way that the current examples are not.

To this end, one of the efforts that aeropropulsion engineers are focusing on is the design of the engine inlet. Both axisymmetric and two-dimensional types are being considered. The two-dimensional candidate is referred to as a bifurcated inlet because it splits the captured mass flow for one engine and initially divides it into two streams. The advantage of such an arrangement over a two-dimensional single-stream inlet (both the Tu-144 and the Concorde are single-stream types) is one of potential length (and thereby weight) reduction. A bifurcated design can be as much as 50% shorter than a single-stream inlet designed for the same captured mass flow. Figure 1a illustrates the essential elements of the bifurcated inlet using a mixed-compression example tested at NASA Lewis Research Center.[1] A combination of oblique shocks and internal compression comprises the upstream supersonic diffuser. This region of the inlet terminates in a normal shock nominally located at the throat or upstream end of the subsonic diffuser. An elaborate bleed system is used to control the boundary-layer and shock-impingement locations in the supersonic diffuser. Vortex generators and a bypass bleed system are used to control boundary-layer development in the subsonic diffuser. Figure 1b is an oblique view of the inlet (looking upstream) as it would appear in a flight configuration mounted under a wing surface. One half of the bifurcated subsonic diffuser is highlighted with heavy lines in Fig. 1b. This type of diffuser is referred to as a transitioning S-diffuser because of the cross-sectional area change (from rectangular to semiannular) and a slight S-shaped centerline curvature.

Like many other problems in engineering, diffuser design is a balance of conflicting requirements. In general terms, subsonic diffusers are designed to supply an airstream to an engine. The properties of this airstream are constrained by the requirements of the engine compressor. Some degree of fluid deceleration, pressure rise, and flow uniformity at the compressor are typically called for. Deceleration of the fluid to the desired velocity requires an increase in the cross-sectional area. If this process is to occur in an efficient manner, the internal boundary layers must not thicken excessively or detach from the flow surfaces. Working against this are the length and cross-sectional geometry requirements of the inlet and con-

Received July 23, 1997; revision received Jan. 12, 1998; accepted for publication Jan. 23, 1998.

*Senior Research Engineer, Aerospace Propulsion Division, 7530 Lucerne Drive, Islander Two, Suite 206. Member AIAA.

†Aerospace Engineer, Inlet Branch, M/S 5–11, 21000 Brookpark Road. Senior Member AIAA.

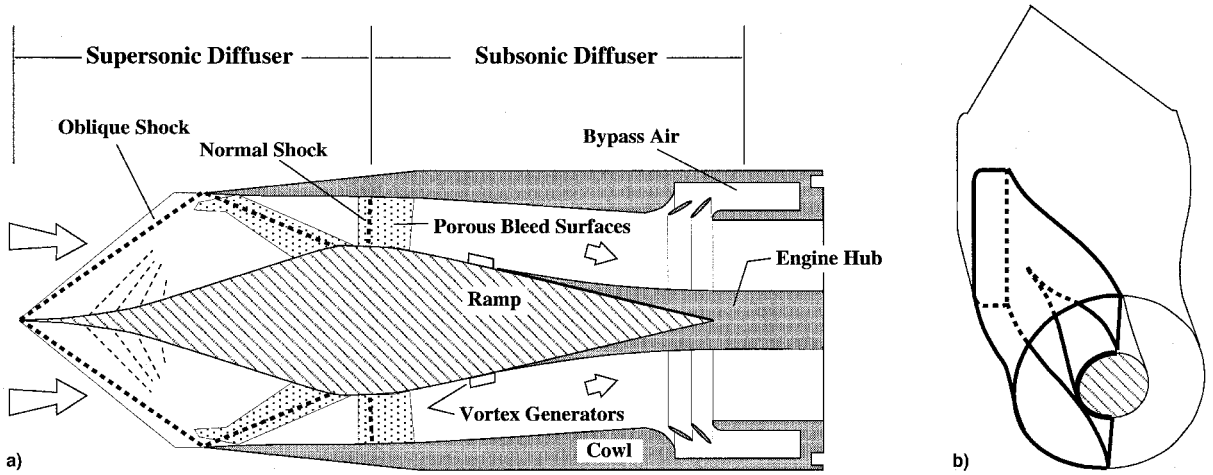

Fig. 1 Bifurcated supersonic inlet.

nected propulsion system. Shortening the diffuser increases the adverse axial pressure gradient and the possibility of global boundary-layer separation; transitions in cross-sectional shape and duct centerline curvature promote the development of secondary flows. Once established, secondary flows have a tendency to accumulate boundary-layer fluid at discrete locations, thereby increasing the possibility of localized flow separation and attendant flow nonuniformity.

Vortex generators are devices used to counter these problems. The concept of using vortex generators to control boundary-layer flows was first developed as a means of enhancing diffuser performance. The earliest studies were conducted by Taylor,[2] Grose and Taylor,[3] and Pearcy.[4] At the most fundamental level, a vortex generator is simply a protrusion into a fluid stream that sheds a vortex (or vortices) into the downstream boundary layer. The basis of boundary-layer control lies in the convective nature of this shed vortex. The vortex mixes the high-energy fluid of the freestream (or duct core flow) with the slower-moving fluid of the boundary layer. The boundary-layer fluid is effectively re-energized and is now more resistant to separation. This mixing mechanism of vortex generator effectiveness is long established. A good description is found in the report of Schubauer and Spangenburg.[5] In addition to promoting fluid mixing, vortex generators may also be used to counter the detrimental effects of secondary flows. This mode of vortex generator effectiveness was recently explored using a diffusing S-duct geometry in studies by Anderson and Levy,[6] Reichert and Wendt,[7] and Anderson and Gibb.[8]

Diffuser performance is quantified in terms of recovery and distortion descriptors. Total pressure recovery is a measure of the efficiency of the diffusion process, whereas total pressure distortion is a measure of the flow uniformity supplied to the engine. In optimizing diffuser performance through a suitable application of vortex generators, we must first determine the balance required between recovery and distortion of our inlet and engine system. Because each vortex generator used represents an energy loss (through device drag, a function of vortex generator frontal area), optimization requires us to use the minimum number (or minimum total frontal area) of vortex generators needed to obtain the required recovery and distortion goals. How one achieves this number and pattern is the essence of the design problem. The large number of geometric parameters in the vortex generator design and vortex generator arrangement (or array) make this problem difficult. Consider Fig. 2, which illustrates an array of common vane-type vortex generators mounted on an internal flow surface. The geometric elements of the individual vortex generators (chord c, span h, angle of attack α, etc.) relate directly to the initial strength and concentration of the shed vortices, and so must be chosen carefully. Also of critical importance is the manner in which the

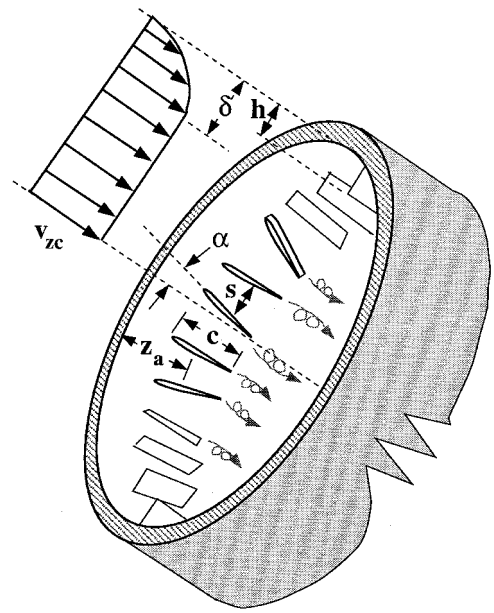

Fig. 2 Many parameters of vortex generator design include elements of the array geometry.

vortices interact downstream. This is partially determined by the axial location of the array z_a, the initial spacing between vortex generators s, and the rotational orientation of the array, i.e., whether vortices are shed counter-rotating or corotating with respect to immediate neighbors. Limited experimental parametric studies have been conducted to develop effective strategies for vortex generator use in a diffusing S-duct[7,9] and a rectangular-to-semiannular diffuser similar to the one illustrated in Fig. 1b.[10] Of greater potential utility is the application of computational fluid dynamics to the optimization problem. In particular, fast diffuser design codes based on solutions to the parabolized (or reduced) Navier–Stokes equations have the ability to run through large parametric ranges in a time- and cost-effective manner.

The objective of this study is to develop a synergistic computational–experimental approach to vortex generator use for a transitioning S-diffuser. The code used is a parabolized code known as RNS3D. It is a modification of the PEPSIG code based on the stream function–vorticity formulation of the reduced Navier–Stokes equations and was originally developed for internal flows on nonorthogonal grids by Levy et al.[11] Experimental measurements are conducted on a corresponding test model. These measurements are meant to calibrate both

the vortex generator model used in the code and the code distortion results, as well as track the losses incurred through vortex generator use. Optimum diffuser performance results are not necessarily achieved by the synthesis described herein, nor can we show that this effort will achieve optimization; but the results obtained demonstrate large improvements and serve as a first step in addressing this difficult design problem.

Tools and Procedures

Diffuser Definition

The rectangular-to-semiannular diffuser used in this study (designated td118) is one of a series of geometrically similar ducts designed by Anderson and Kapoor.[12] If the o.d. of the annular exit cross section is D, then the overall axial length-to-diameter ratio is $L/D = 2.0$. The exit-to-inlet cross-sectional area ratio is $A_e/A_i = 1.51$. Figure 3 provides three views of the td118 diffuser and assists in the following mathematical description.

The td118 diffuser consists of a rectangular-to-semicircular outer shell plus a tapered, half cylindrically shaped centerbody, located at midspan on the floor of the outer shell. The diffuser outer shell maintains a width of $D = 25.4$ cm over its axial length $L = 50.8$ cm. When viewed in profile we note that the line that defines the top center of the duct is straight (no curvature in the x_1, x_3 plane). The floor of the outer shell is of width D and has no curvature in the x_2, x_3 plane. The coordinates for the centerline of the outer shell floor are

$$\frac{x_{icl}}{D} = \sum_{j=0}^{5} c_{i,j} \left(\frac{x_1}{D}\right)^j, \qquad i = 1, 2, 3 \tag{1}$$

The coordinate system definitions are provided in Fig. 3. The duct cross section is defined by a superellipse in a plane perpendicular to the centerline of Eq. (1). The triple (x_4, x_5, x_6) represents the orthogonal coordinate system (Fig. 3). The equation for the duct cross section is

$$\left(\frac{2x_5/D}{B_4}\right)^{B_6} + \left(\frac{2x_6/D}{B_5}\right)^{B_6} = 1 \tag{2}$$

and the equation for the centerbody cross-sectional shape is

$$\left(\frac{2x_5/D}{B_7}\right)^{B_6} + \left(\frac{2x_6/D}{B_8}\right)^{B_6} = 1 \tag{3}$$

where the B_i are defined by equations having the form of Eq. (1):

$$B_i = \sum_{j=0}^{5} c_{i,j} \left(\frac{x_1}{D}\right)^j, \qquad i = 4, \ldots, 8 \tag{4}$$

The constants $c_{i,j}$ from Eqs. (1) and (4) are listed in Table 1.[13]

Experimental Facility

Experimental measurements of the td118 diffuser flowfield were made at NASA Lewis Research Center using the Internal Fluid Mechanics Facility (IFMF). This facility was designed to support the research of a variety of internal flow configurations and is described in detail by Porro et al.[14] The facility in the vicinity of the test section, as it is assembled for this test, is illustrated in Fig. 4. Laboratory air at atmospheric conditions flows into a large settling plenum. Flow-conditioning elements (honeycombs and screens) are located in this plenum and are used to reduce the turbulence levels of the incoming airstream. A pair of contraction ducts accelerates the flow supplied to a roughly constant flow area spool section having a cross section with the same dimensions as the diffuser throat. Static pressure instrumentation in the spool section provides the reference throat Mach number for the diffuser model located immediately downstream. Cross-plane measurements of diffuser exit plane total pressure are acquired by two translating rakes of five-hole probes (three tips per rake). These rakes are similar to the rake described in the report of Wendt and Reichert.[15] The two rakes follow radial survey lines 90 deg apart and the grid resolution is $\Delta r = 4$ mm and $\Delta\theta = 5$ deg in the semiannular diffuser exit plane. Upon exiting the instrumentation duct the airstream is routed through a flexible steel hose to an exhaust plenum that is continuously evacuated.

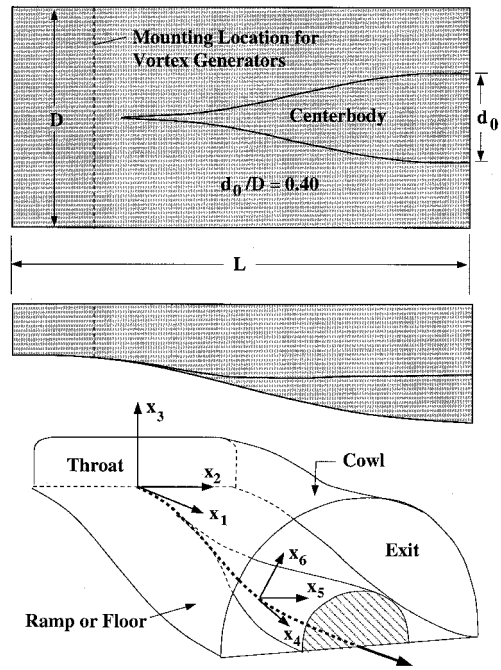

Fig. 3 Three views of the td118 diffuser.

Total pressure results originate from the five-hole probe measurements acquired with an electronically scanned transducer system. The transducer's manufacturer states a measurement uncertainty of ± 0.05 KPa. Uncertainty in the pressure measurement data is used to derive total pressure result uncertainty following the procedure outlined by Reichert and Wendt.[16] Uncertainty in the total pressure ratio is approximately $\pm 1\%$.

The reference throat Mach number for this test is 0.79. The mass flow rate at this condition is approximately 3 kg/s. The boundary layer at the throat is turbulent and uniform in thickness about the throat circumference with $\delta_{ref}/D \approx 0.01$. The throat Reynolds number, based on the dimension D, is approximately 4×10^6. The exit plane core Mach number has a nominal value of about 0.45.

The delta-wing-like vortex generators applied in this study are illustrated in Fig. 5. These devices are similar to the tapered fin first examined in the report of Schubauer and Spangenburg.[5] Each vortex generator will shed a single trailing axial vortex when its leading edge is aligned with the flow as shown in Fig. 5. Three geometrically similar tapered fins, differing only in scale, are used. The chord lengths are listed in Fig. 5.

Computational Code

The RNS3D code was developed primarily as a design and analysis tool to efficiently compute internal subsonic flows. It has been used in previous efforts to resolve complex three-dimensional flows in various aerospace propulsion-related applications, and requires significantly less computational time than comparable full Navier–Stokes (FNS) codes.[12,17] The simplicity of the RNS3D code results, in part, from a decomposition of the velocity vector into primary and secondary components; it also neglects viscous and thermal diffusion in the streamwise direction. The primary velocity is obtained from

Table 1 $C_{i,j}$ constants in Eqs. (1) and (4)

	j					
i	0	1	2	3	4	5
			A. $0 \leq x_1/D < 0.5$			
1	0.00000000	1.0000000	0.00000000	0.00000000	0.00000000	0.00000000
2	0.00000000	0.00000000	0.00000000	0.00000000	0.00000000	0.00000000
3	0.00000000	0.00000000	0.00000000	−0.08807312	0.03802742	−0.00330274
4	1.0000000	0.00000000	0.00000000	0.00000000	0.00000000	0.00000000
5	0.43633200	0.00000000	0.00000000	0.08807312	−0.03302742	0.00330274
6	20.000000	−20.5000000	8.62500000	−1.59375000	0.10937500	0.00000000
7	0.00000000	0.00000000	0.00000000	0.00000000	0.00000000	0.00000000
8	0.00000000	0.00000000	0.00000000	0.00000000	0.00000000	0.00000000
			B. $0.5 \leq x_1/D \leq 2.0$			
1	0.00000000	1.0000000	0.00000000	0.00000000	0.00000000	0.00000000
2	0.00000000	0.00000000	0.00000000	0.00000000	0.00000000	0.00000000
3	0.00000000	0.00000000	0.00000000	−0.08807312	0.03802742	−0.00330274
4	1.0000000	0.00000000	0.00000000	0.00000000	0.00000000	0.00000000
5	0.43633200	0.00000000	0.00000000	0.08807312	−0.03302742	0.00330274
6	20.000000	−20.5000000	8.62500000	−1.59375000	0.10937500	0.00000000
7	−0.2305185	0.78814810	−0.98518520	0.54185190	0.12314810	0.00985185
8	−0.2305185	0.78814810	−0.98518520	0.54185190	0.12314810	0.00985185

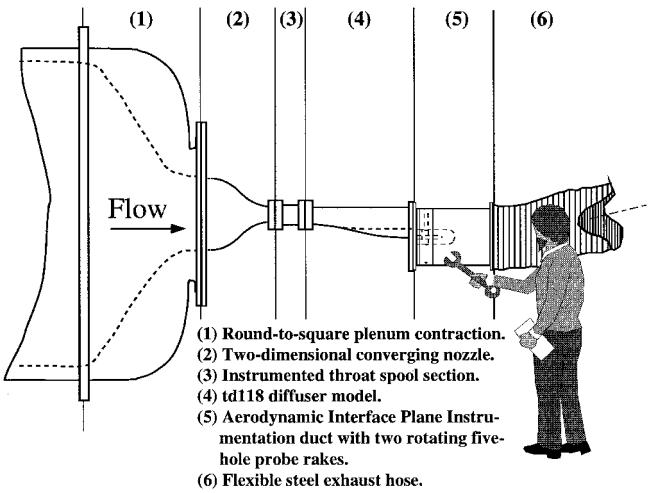

Fig. 4 Diffuser test rig.

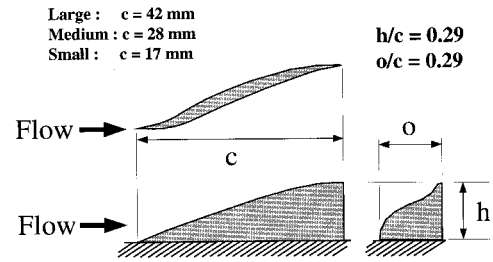

Fig. 5 Geometry of the tapered fin vortex generator.

the solution of the streamwise momentum equation and the secondary velocities are solved via a vorticity and stream function formulation. These equations are approximated with finite differences and solved by forward spatial marching.

The utility of RNS3D in this study is derived from its ability to model the convective effects of vortex generators on the diffuser flowfield, without actually including the vortex generator geometry in the diffuser computational grid. The convective model used takes advantage of the vorticity and stream function formulation of the code's governing equations. The shed vortex is modeled by adding a source term to the vorticity transport equation at each grid point in the cross-plane of the vortex generator. The strength of the source term is determined by assuming a circulation profile for the shed vortex, which, in turn, is a function of the vortex generator chord length, impinging flow conditions, and radial distance from the vortex generator. More information on this vortex generator modeling procedure may be found in the reports of Kunik[18] and Anderson and Gibb.[19]

The computational mesh used here was developed by Anderson and Kapoor.[12] Because the duct is symmetric, only half of the duct, a 90-deg section, was computed. The transverse cross-planes are perpendicular to the duct centerline and have 99 radial and 49 circumferential points each. In the streamwise (x_1) direction a constant cross-sectional area duct of length $\Delta x_1/D = 0.5$ is added at either end of the diffuser to satisfy the boundary-condition requirements of the code. Streamwise grid resolution is $\Delta x_1/D = 0.013$ in the diffuser and $\Delta x_1/D = 0.025$ in the two constant cross-sectional area ducts. The resulting grid has a total of 201 × 99 × 49 points. Flowfield boundary conditions are matched to the previously discussed experimental conditions.

Results

Diffuser Performance Descriptor Definition

The diffuser performance descriptors evaluated in this study are area-averaged total pressure recovery and circumferential distortion intensity. These descriptors are determined on a cross-plane grid that covers the entire circular engine face. Figure 6 shows how flowfield symmetry is used in these evaluations. As an example, the upper half-circle in Fig. 6 illustrates the experimental survey grid used in most test cases. Mirror image symmetry through the line l_1 is always assumed. For computations and some experimental data, mirror image symmetry through the line l_2 is also used. Because of the geometry of the duct and vortex generator arrays, symmetry through l_2 is, in principle, appropriate for all test cases considered here. An area average of a quantity β over an annular section of angular extent $\Delta\theta = b - a$ and radial extent $\Delta r = d - c$ is defined as

$$\bar{\beta}(a, b: c, d) = \frac{\int_a^b \int_c^d \beta r \, dr \, d\theta}{\int_a^b \int_c^d r \, dr \, d\theta} \tag{5}$$

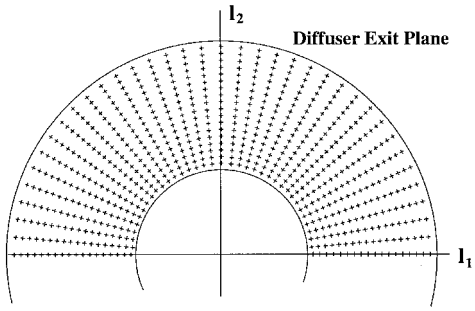

Fig. 6 Experimental grid at the diffuser exit showing lines of flowfield symmetry.

Area-averaged total pressure recovery, or AATPR, is defined from Eq. (5) by letting $\beta = p_t/p_{t\text{ref}}$, $a = 0$, $b = 2\pi$, $c = d_0/2$, and $d = D/2$. Thus we can write

$$\text{AATPR} = \frac{\bar{p}_t}{p_{t\text{ref}}}\left(0, 2\pi: \frac{d_0}{2}, \frac{D}{2}\right) \equiv \frac{\bar{p}_t}{p_{t\text{ref}}} \tag{6}$$

In a similar fashion, the circumferential distortion DC60 is defined as

$$\text{DC60} = \frac{\bar{p}_t\left(0, 2\pi: \frac{d_0}{2}, \frac{D}{2}\right) - \bar{p}_t\left(\theta, \theta + \frac{\pi}{3}: \frac{d_0}{2}, \frac{D}{2}\right)_{\min}}{\bar{q}\left(0, 2\pi: \frac{d_0}{2}, \frac{D}{2}\right)} \tag{7}$$

where $\bar{p}_t[\theta, \theta + (\pi/3): (d_0/2), (D/2)]_{\min}$ is the minimum value of $\bar{p}_t[\theta, \theta + (\pi/3): (d_0/2), (D/2)]$ occurring over the entire annular cross-plane.

The radial profile of circumferential distortion intensity, termed "sixty-degree ring sector distortion" or 60DRSD is defined for a ring of radius r_i and thickness dr:

$$\text{60DRSD} = \frac{\bar{p}_t(a, b: c, d) - \bar{p}_t[\theta, \theta + (\pi/3): c, d]_{\min}}{\bar{p}_t(a, b: c, d)} \tag{8}$$

where $a = 0$, $b = 2\pi$, $c = r_i - dr/2$, $d = r_i + dr/2$, and $\bar{p}_t[\theta, \theta + (\pi/3): c, d]_{\min}$ is the minimum value of $\bar{p}_t[\theta, \theta + (\pi/3): c, d]$ occurring over the full circular ring. As an example, the experimental grid illustrated in Fig. 6 is naturally divided into 18 such rings.

Baseline Diffuser

The term "baseline" refers to a td118 diffuser model without a surface-mounted vortex generator array. In the experimental program, two td118 models were tested with and without vortex generators. One model was constructed from plastic using a laser-stereolithography technique. The other model was milled from a block of aluminum alloy. Under normal operating conditions a pressure differential existed across the wall of the diffuser model. The plastic diffuser was found to undergo a small amount of wall deflection because of this pressure loading. The deflection was greatest near the diffuser throat (where the Mach number is highest) and produced a thin region of vortical flow separation on the ramp surface of the plastic model. In the metal diffuser, which suffered no measurable deflection, the ramp boundary layer stagnated, but did not separate. Figure 7 compares ramp surface flow streamlines for both plastic and metal diffusers. This illustration was obtained from surface oil-flow patterns. The region of separated or stagnated flow on the ramp was observed to be almost entirely suppressed when vortex generators were applied.

Flow separation in the plastic diffuser produced thicker boundary layers on the ramp and centerbody surfaces. This can be seen in Figs. 8a and 8b, which compare baseline exit

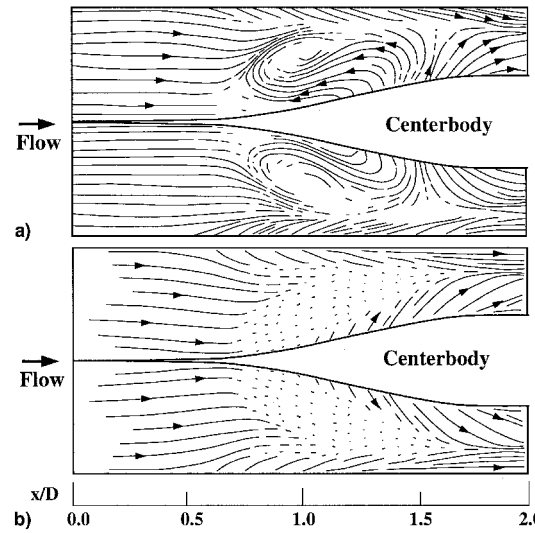

Fig. 7 Baseline ramp surface streamlines: a) plastic duct and b) aluminum duct.

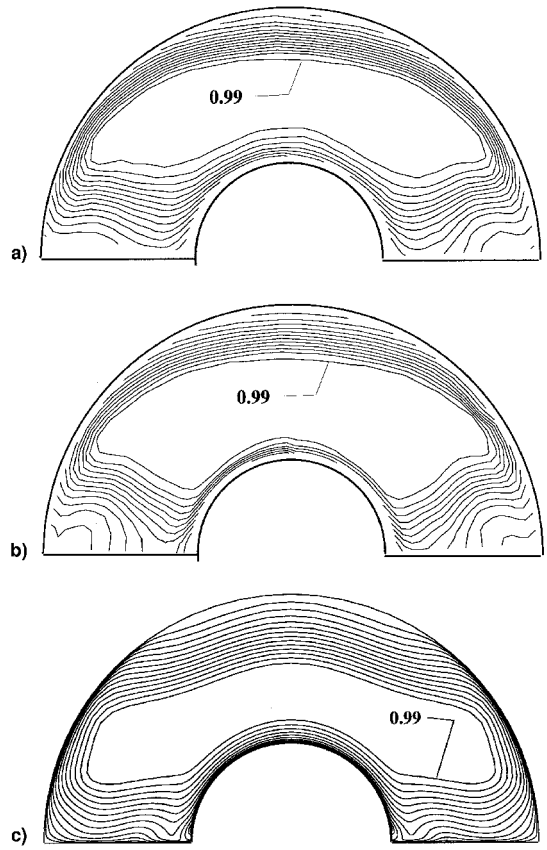

Fig. 8 Contour plots of total pressure ratio ($p_t/p_{t\text{ref}}$) in the exit plane of the diffuser: a) plastic, b) aluminum, and c) RNS3D (contour increment = 0.01).

plane total pressure contours of the plastic and metal diffusers, respectively. The thicker boundary layers are responsible for a degradation in the performance of the plastic model:

$$\begin{aligned}\text{AATPR, DC60} &= 0.944, 0.290 \text{ (plastic)}\\ \text{AATPR, DC60} &= 0.954, 0.267 \text{ (metal)}\end{aligned} \tag{9}$$

Figure 8c shows the total pressure contours from the RNS3D calculation; the corresponding performance descriptors are

$$\text{AATPR, DC60} = 0.953, 0.065 \text{ (RNS3D)} \tag{10}$$

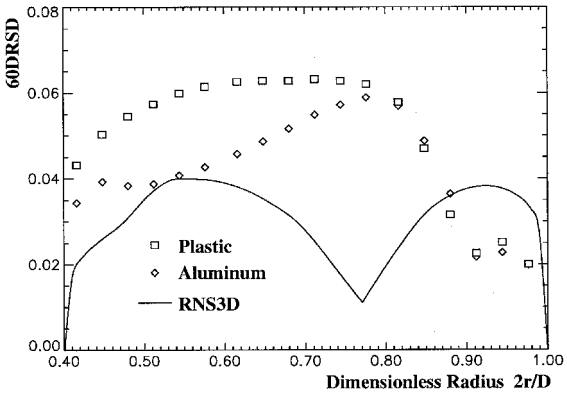

Fig. 9 Profiles of circumferential distortion of the baseline diffuser.

Figure 9 compares the corresponding radial profiles of 60DRSD. In general terms, the code overpredicts the cowl boundary-layer thickness and somewhat underpredicts the ramp boundary-layer thickness. This is evident in the distinct two-lump pattern produced by the calculation; the first left-hand-side (LHS) lump is produced primarily by the ramp boundary layer, and the second right-hand-side (RHS) lump originates from the cowl boundary layer.

Vortex Generator Design Sequence

The overall objective of vortex generator use in the td118 diffuser is to reduce the circumferential distortion of the duct while minimizing the drag-related recovery losses. This process was carried out in two parts:

1) The baseline total pressure contours (Figures 8a–8c) were carefully studied. We then asked ourselves the question: "What changes in these patterns would result in lower values of circumferential distortion?" Several concepts were considered. These concepts were implemented using the considerable convective influence of the medium or large vortex generators. Five trials were conducted in the plastic diffuser. In addition to overall screening, the results were also used to calibrate the vortex generator model in the code and to establish a means of performance comparison between computational and experimental results. This means of comparison is the radial profile of 60DRSD. Of the five trials conducted, the one producing the minimum amount of DC60 was chosen for further refinement.

2) In the second part our aim was to minimize the recovery losses. Using the pattern having the minimum value of DC60 established earlier, each large vortex generator was replaced with a corotating pair or triple composed of small vortex generators. Proper placement of these vortex generators was established using the code. Many computational trials were conducted, and the two refined patterns that produced the most favorable profiles of 60DRSD were tested experimentally in the aluminum diffuser.

The vortex generator array was designed for (and mounted at) a single axial location: $x_1/D = 0.575$ downstream of the diffuser throat (Fig. 3).

Figure 10 illustrates the exit plane total pressure results of the five pattern trials conducted experimentally in the plastic diffuser. The RHS of each contour plot illustrates the experimental results and the LHS illustrates the computational mimic. Experimental values of AATPR and DC60 are listed with each corresponding contour plot.

In the geometry of the td118 duct, the diffusion is provided by the ramp floor turning down away from the stream. Thus, our first flow-control concept was to use two pairs of downflow vortices on the ramp to assist in turning the stream to follow the surface contour of the duct. The term downflow vortex pair refers to the convective action of the shed vortices. The fluid between the vortices in the pair is convected toward

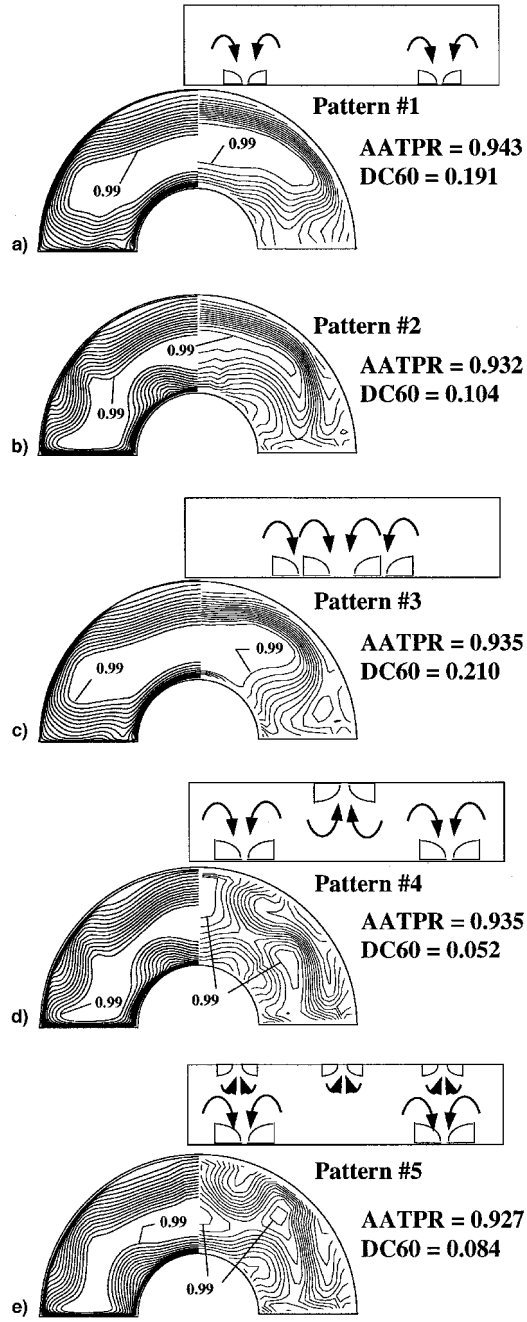

Fig. 10 Contours of total pressure ratio for the trial vortex generator patterns in the plastic diffuser (contour increment = 0.01).

the wall (the downward direction). Each downflow pair was centered on the two streamwise channels created by the diffuser cowl and centerbody surfaces. Pattern 1 (Fig. 10a) used medium-sized vortex generators, and pattern 2 (Fig. 10b) used large vortex generators. Each pattern demonstrates an effective thinning of the ramp boundary layer.

The second flow-control concept tested is related to the perceived beneficial action of the centerbody on the diffuser flowfield. The centerbody is designed to prevent the duct from overdiffusing and the ramp boundary layer from separating. Vortex generator pattern 3 (Fig. 10c) uses two corotating pairs of large vortex generators to produce a region of strong downflow on the ramp centerline for an enhanced centerbody effect. The resulting pattern did not significantly reduce the circumferential distortion.

The third flow-control concept is similar to the first, but also includes a downflow vortex pair (or pairs) on the cowl surface.

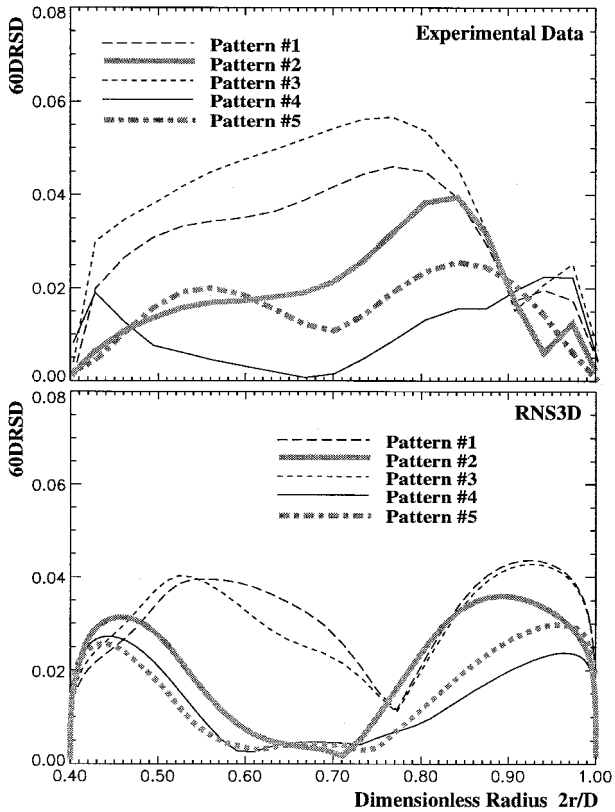

Fig. 11 Comparison of 60DRSD profiles of the five trial vortex generator arrays.

Pattern 4 (Fig. 10d) has three pairs of large vortex generators (two on the ramp surface as in pattern 2, and one on the cowl centerline). Pattern 5 (Fig. 10e) has five pairs of vortex generators (two large pairs on the ramp surface as in pattern 2, and three medium-sized pairs equally spaced on the cowl surface). The downflow vortex pairs placed on the cowl surface were found to effectively thin the cowl boundary layer.

Figure 11 compares the five plastic duct experimental profiles of 60DRSD to the computational profiles. As in the baseline case, the experimental and computational profiles do not have corresponding shapes; however, the trend in distortion reduction (from patterns 1 to 5) is reproduced in the computational results.

Of the 5 trials conducted, pattern 4 represented the best strategy for minimizing circumferential distortion. Comparison of pattern 4 to the plastic diffuser baseline shows an 82% reduction in DC60 paid for with a 1% loss in AATPR. A large penalty in drag-related losses was tied to the use of large vortex generators in pattern 4. To gain back a portion of the total pressure recovery performance lost, we next replaced each large vortex generator in pattern 4 with a set of small corotating vortex generators. Double and triple sets were considered. The proper spacing between the vortex generators was determined by running various trials with RNS3D and comparing the resulting profiles of 60DRSD. The spacing ratio of pattern 4 was $s/D = 0.175$, where s is the distance between adjacent trailing-edge tips of the tapered fin vortex generators. The optimum spacing for small double sets was determined to be $s/D = 0.042$, and for small triple sets $s/D = 0.031$. The resulting vortex generator arrays, patterns 6 and 7, were tested in the aluminum diffuser. The results are illustrated in Fig. 12. Comparison of pattern 6 to the aluminum diffuser baseline indicates a 59% reduction in DC60 paid for with a 0.3% loss in AATPR. Figure 13 plots the corresponding experimental and computational profiles of 60DRSD for the results obtained using vortex generators in the aluminum diffuser.

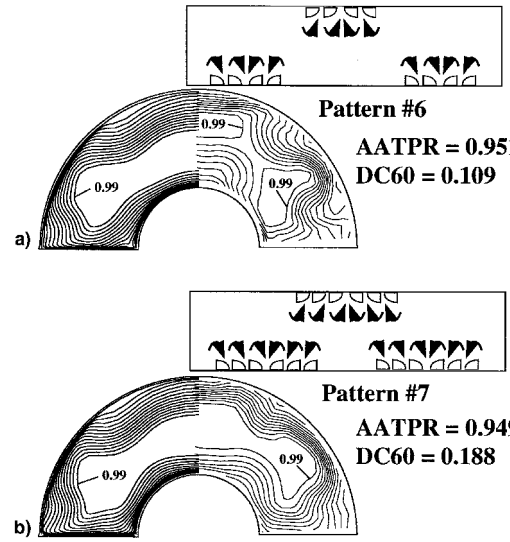

Fig. 12 Exit plane contours of total pressure ratio for vortex generator pattern refinement in the aluminum diffuser: a) doubles and b) triples (contour increment = 0.01).

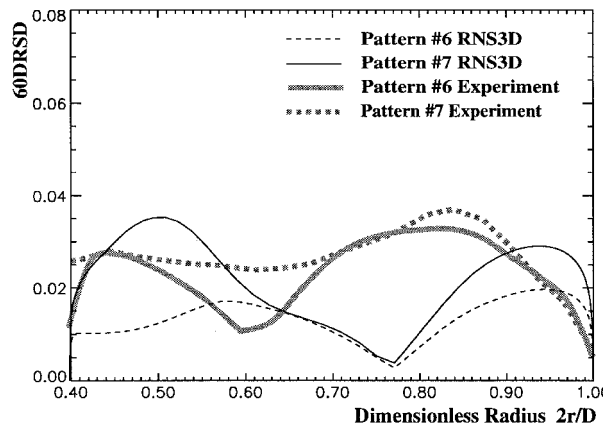

Fig. 13 Comparison of experimental and computational profiles of 60DRSD for vortex generator pattern refinement in the aluminum diffuser.

A comparison of the baseline flowfields in Fig. 8 to the vortex generator-influenced flowfields of Figs. 10 and 12 reveals the considerable convective power of the vortices shed from the tapered fins. It is important to emphasize that the improvements in distortion behavior represented by these figures were achieved with only the simplest understanding and representation of the convective nature of the shed vortices. The maximum benefit possible, i.e., optimization, will likely be achieved only with a deeper understanding of internal flows. This applies equally to the flow problems generated unintentionally within the duct and the flow induced by devices (such as vortex generators) used to counter them. The simple procedure and results described here should provide further incentive for such efforts.

Summary

Computational and experimental methods were used synergistically to develop a beneficial vortex generator design for the td118 transitioning S-shaped diffuser. The most beneficial configurations are those that minimize both total pressure distortion and losses. The RNS3D code was used to screen several vortex generator patterns to determine the vortex generator placement that produced minimum distortion in the diffuser exit plane flowfield. Experimental measurements were taken to find the vortex generator size required to minimize total

pressure losses. The best result achieved a 59% reduction in DC60 distortion with only a 0.3% reduction in total pressure recovery.

Acknowledgments

The authors wish to acknowledge Bernie Anderson and Kamlesh Kapoor for their efforts in producing the baseline grid and flow solution. Charlie Towne provided valuable assistance in debugging the vortex generator subroutines in the RNS3D code. Bruce Reichert and Jeff Foster assisted in the design, construction, and operation of the test facilities. Finally, a special thank you to B. Darby and M. Binchy for their helpful insights.

References

[1]Wasserbauer, J. F., Meleason, E. T., and Burstadt, P. L., "Experimental Investigation of the Performance of a Mach 2.7 Two Dimensional Bifurcated Duct Inlet with 30 Percent Internal Contraction," NASA TM 106728, May 1996.

[2]Taylor, H. D., "Application of Vortex Generator Mixing Principles to Diffusers. Concluding Report," United Aircraft Corp. Research Dept., Rept. R-15064-5, East Hartford, CT, Dec. 1948.

[3]Grose, R. M., and Taylor, H. D., "Theoretical and Experimental Investigation of Various Types of Vortex Generators," United Aircraft Corp. Research Dept., Rept. R-15362-5, East Hartford, CT, March 1954.

[4]Pearcy, H. H., "Shock-Induced Separation and Its Prevention by Design and Boundary Layer Control," *Boundary Layer and Flow Control*, edited by G. V. Lachmann, Vol. 2, Pergamon, New York, 1961, pp. 1166–1344.

[5]Schubauer, G. B., and Spangenburg, W. G., "Forced Mixing in Boundary Layers," *Journal of Fluid Mechanics*, Vol. 8, Pt. 1, 1960, pp. 10–31.

[6]Anderson, B. H., and Levy, R., "A Design Strategy for the Use of Vortex Generators to Manage Inlet-Engine Distortion Using Computational Fluid Dynamics," AIAA Paper 91-2474, June 1991.

[7]Reichert, B. A., and Wendt, B. J., "Improving Curved Subsonic Diffuser Performance with Vortex Generators," *AIAA Journal*, Vol. 34, No. 1, 1996, pp. 65–72.

[8]Anderson, B. H., and Gibb, J., "Vortex Generator Installation Studies on Steady State and Dynamic Distortion," AIAA Paper 96-3279, July 1996.

[9]Reichert, B. A., and Wendt, B. J., "An Experimental Investigation of S-Duct Flow Control Using Arrays of Low Profile Vortex Generators," AIAA Paper 93-0018, Jan. 1993.

[10]Brown, A. C., Nawrocki, H. F., and Paley, P. N., "Subsonic Diffusers Designed Integrally with Vortex Generators," *Journal of Aircraft*, Vol. 5, No. 3, 1968, pp. 221–229.

[11]Levy, R., Briley, W. R., and McDonald, H., "Viscous Primary/Secondary Flow Analysis for Use with Nonorthogonal Coordinate Systems," AIAA Paper 83-0556, Jan. 1983.

[12]Anderson, B. H., and Kapoor, K., "A Study on Bifurcated Transitioning S-Ducts for High Speed Inlet Application," AIAA Paper 94-2812, June 1994.

[13]Foster, J., Okiishi, T. H., Wendt, B. J., and Reichert, B. A., "Study of Compressible Flow Through a Rectangular-to-Semiannular Transition Duct," NASA CR 4660, April 1995.

[14]Porro, A. R., Hingst, W. R., Wasserbauer, C. A., and Andrews, T. B., "The NASA Lewis Research Center Internal Fluid Mechanics Facility," NASA TM 105187, Sept. 1991.

[15]Wendt, B. J., and Reichert, B. A., "An Inexpensive and Effective Five-Hole Probe Rake," *Experiments in Fluids*, Vol. 19, Aug. 1995, pp. 295, 296.

[16]Reichert, B. A., and Wendt, B. J., "A New Algorithm for Five-Hole Probe Calibration, Data Reduction, and Uncertainty Analysis," NASA TM 106458, March 1994.

[17]Towne, C. E., "Computation of Viscous Flow in Curved Ducts and Comparison with Experimental Data," NASA TM 83548, Jan. 1984.

[18]Kunik, W. G., "Application of a Computational Model for Vortex Generators in Subsonic Internal Flows," AIAA Paper 86-1458, June 1986.

[19]Anderson, B. H., and Gibb, J., "Study on Vortex Generator Flow Control for the Management of Inlet Distortion," *Journal of Propulsion and Power*, Vol. 9, No. 3, 1993, pp. 422–430.